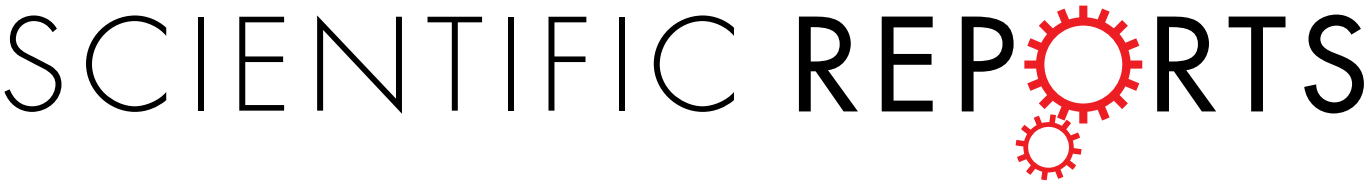

OPEN

Low-Energy Amorphization of $Ti_1Sb_2Te_5$ Phase Change Alloy Induced by $TiTe_2$ Nano-Lamellae

Received: 16 February 2016
Accepted: 08 July 2016
Published: 29 July 2016

Keyuan Ding[1,2], Feng Rao[1], Shilong Lv[1], Yan Cheng[1], Liangcai Wu[1] & Zhitang Song[1]

Increasing SET operation speed and reducing RESET operation energy have always been the innovation direction of phase change memory (PCM) technology. Here, we demonstrate that ~87% and ~42% reductions of RESET operation energy can be achieved on PCM cell based on stoichiometric $Ti_1Sb_2Te_5$ alloy, compared with $Ge_2Sb_2Te_5$ and non-stoichiometric $Ti_{0.4}Sb_2Te_3$ based PCM cells at the same size, respectively. The $Ti_1Sb_2Te_5$ based PCM cell also shows one order of magnitude faster SET operation speed compared to that of the $Ge_2Sb_2Te_5$ based one. The enhancements may be caused by substantially increased concentration of $TiTe_2$ nano-lamellae in crystalline $Ti_1Sb_2Te_5$ phase. The highly electrical conduction and lowly thermal dissipation of the $TiTe_2$ nano-lamellae play a major role in enhancing the thermal efficiency of the amorphization, prompting the low-energy RESET operation. Our work may inspire the interests to more thorough understanding and tailoring of the nature of the $(TiTe_2)_n(Sb_2Te_3)_m$ pseudobinary system which will be advantageous to realize high-speed and low-energy PCM applications.

Non-volatile phase change memory (PCM), as one of the promising candidates, has great potential to serve as a storage class memory (SCM) to mitigate the widened performance mismatch between dynamic random access memory (DRAM) and non-volatile NAND Flash memory[1,2]. In the PCM cell, a chalcogenide material, for example, $Ge_2Sb_2Te_5$, can be switched between the crystalline (c-) and amorphous (a-) phases, corresponding to the SET and RESET states[3,4], respectively. The big resistance contrast of such two states is utilized for storing "0" and "1" data states. The RESET operation refers to an amorphization procedure which melts the c-phase and subsequently quenches it into a-phase by applying a short intense electrical pulse on the PCM cell. Conversely, a longer pulse of lower intensity for SET operation can heat the a-phase to a temperature between crystallization temperature (T_c) and melting point (T_m) to obtain the c-phase. To achieve high density SCM application, scaling capability of the PCM cell is largely limited by its high RESET current or energy[5] for which the premature degradation of the switching material or the thermal disturbance among nearest cells would happen and cause reliability and endurance issues[6].

Since the slow SET speed and high RESET power remain to be important limitations for developing DRAM-like PCM, our previous work demonstrated at least one order of magnitude faster SET speed and as low as one-fifth of the RESET current and energy on a $Ti_{0.4}Sb_2Te_3$ based PCM cell compared to those of the $Ge_2Sb_2Te_5$ based cell with the same size[7]. The stable c-$Ti_{0.4}Sb_2Te_3$ alloy has the nano-scale phase separated morphology that hexagonal (HEX) Sb_2Te_3 and HEX-$TiTe_2$ crystals coexist[8]. The triple-layered $TiTe_2$ crystal lamellae locate adjacent to the quintuple-layered Sb_2Te_3 grains, while there are also some Ti atoms penetrate into Sb_2Te_3 lattice by occupying Sb sites and constructing Ti-centered octahedrons with surrounding Te atoms[8]. Such $TiTe_2$ lamellae along with the Ti-centered octahedrons can preserve their ordering configurations even after high temperature RESET operations, which is believed to be responsible for the performance boost of the $Ti_{0.4}Sb_2Te_3$ based PCM cell[7,8].

The influence of Ti doping content (x) on the phase change properties of $Ti_xSb_2Te_3$ materials was also studied[9,10]. Although increasing Ti content can enhance 10-year data retention, reduce the volume change upon phase transition, improve interfacial adhesion ability, excessive Ti content ($x \approx 0.56$, ~10.1 at.%) causes Ti segregation which leads to poor endurance characteristic of the PCM cell[9,10]. This phenomenon may correlate to a low solid solubility of Ti atoms in the HEX-Sb_2Te_3 lattice, where only limited number of Ti-centered octahedrons could

[1]State Key Laboratory of Functional Materials for Informatics, Shanghai Institute of Micro-system and Information Technology, Chinese Academy of Sciences, Shanghai 200050, China. [2]University of the Chinese Academy of Sciences, Beijing 100080, China. Correspondence and requests for materials should be addressed to F.R. (email: fengrao@mail.sim.ac.cn)

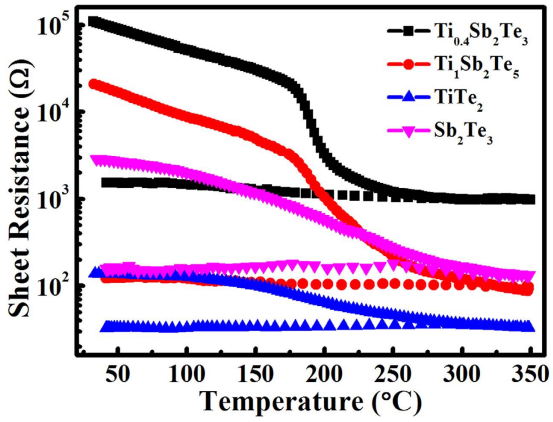

Figure 1. The sheet resistance (R_s) as a function of *in situ* annealing temperature for the $TiTe_2$, Sb_2Te_3, $Ti_{0.4}Sb_2Te_3$, and $Ti_1Sb_2Te_5$ films. The 150 nm thick films deposited on the SiO_2/Si (1 0 0) substrate are measured with the *in situ* heating rate of 10 °C/min.

dispersedly distribute inside the quintuple-layered building blocks so as to preserve the ordering configuration[8]. To inhibit the Ti precipitation after repeated RESET-SET operations, it would be worthwhile to try to concomitantly raise the Te content of the non-stoichiometric $Ti_xSb_2Te_3$ materials. Thus, in this paper, we show the better electrical phase change properties based on a stoichiometric $Ti_1Sb_2Te_5$ material. It is like a pseudobinary compound with 1 : 1 ratio of $TiTe_2$ and Sb_2Te_3 components. Even containing higher Ti content (12.5 at.%), the $Ti_1Sb_2Te_5$ based PCM cell has superior endurance characteristic over the $Ti_{0.56}Sb_2Te_3$ based one. In addition, without significantly sacrificing the SET speed, the RESET energy of the $Ti_1Sb_2Te_5$ based PCM cell is further lowered by 42∼47% compared to the $Ti_{0.4}Sb_2Te_3$ based one. We argue that the richer concentration of $TiTe_2$ lamellae in c-$Ti_1Sb_2Te_5$ plays a major role in decreasing the RESET energy, meanwhile the lack of Ti-centered octahedrons resided in the quintuple-layered Sb_2Te_3 lattice may slow down the nucleation rate, however the increasing $TiTe_2$ lamellae can act as structure-ordering template to enhance the crystal growth rate[11]. Accordingly, we believe that $Ti_1Sb_2Te_5$ material is promising for realizing DRAM-like PCM application once advanced fabrication techniques being applied to further shrink the device dimension.

Figure 1 shows the temperature-dependent sheet resistance (R_s) curves of as deposited $TiTe_2$, Sb_2Te_3, $Ti_{0.4}Sb_2Te_3$, and $Ti_1Sb_2Te_5$ films upon *in situ* annealing with a heating rate of 10 °C/min. As the annealing temperature increases, a continuous decrease in R_s is observed for each film. Due to the partial crystallization during the sputtering process, compared to $Ti_{0.4}Sb_2Te_3$ and $Ti_1Sb_2Te_5$ films, both $TiTe_2$ and Sb_2Te_3 films have smaller initial R_s and present a smooth decrement in R_s. By comparison, one can observe the sudden drop in R_s occurs for $Ti_{0.4}Sb_2Te_3$ and $Ti_1Sb_2Te_5$ films when the temperature reaches T_c (both around 186 °C)[9]. The decrease in R_s with increasing temperature just before the onset of the crystallization indicates a semiconductor-like behavior. The temperature dependence for the R_s in a semiconductor can be expressed by $R_s = R_{s0}\exp(-E_\sigma/kT)$[12], where R_{s0} is a pre-exponential factor and E_σ is the activation energy for electrical conduction. The fitting results of E_σs of $Ti_{0.4}Sb_2Te_3$ and $Ti_1Sb_2Te_5$ are 0.11 eV and 0.13 eV, respectively. The activation energy of electrical transport is simply determined by half of the band gap $E_\sigma = E_G/2 + \Delta E$, where $E_G/2$ is the distance from the Fermi level to the conduction band and ΔE is the depth of the trap states[13]. In the case of intrinsic conduction with equal amounts of electrons and holes, the Fermi level is situated at the middle of the band gap. Thus we can roughly estimate the optical band gaps (E_{OP}s) of a-$Ti_{0.4}Sb_2Te_3$ and a-$Ti_1Sb_2Te_5$ to be ∼0.22 eV and ∼0.26 eV, respectively, both of which are quite smaller than that of a-$Ge_2Sb_2Te_5$ (∼0.70 eV)[14]. Because the carrier density inside the semiconductor is proportional to $\exp(-E_G/2kT)$, where E_G is the electrical band gap which is roughly identical to the E_{OP}, a decrease in the band gap as the temperature approaching to the T_c will lead to the generation of a large number of carriers, which makes a major contribution to the quick drop in film resistivity[14]. On this view, one may roughly estimate that a-$Ti_{0.4}Sb_2Te_3$ and a-$Ti_1Sb_2Te_5$ could have quite faster crystallization (resistivity decrement) speed than that of a-$Ge_2Sb_2Te_5$, and a-$Ti_{0.4}Sb_2Te_3$ could be a little quicker than a-$Ti_1Sb_2Te_5$.

Figure 2a compares the SET speed of $Ge_2Sb_2Te_5$, $Ti_{0.4}Sb_2Te_3$, and $Ti_1Sb_2Te_5$ based PCM cells with the same size (BEC $D = 190$ nm), which has the same trend as aforementioned estimation. As the magnitude of applied voltage pulse reaches 1.3 V and 1.5 V, respectively, both the $Ti_{0.4}Sb_2Te_3$ and $Ti_1Sb_2Te_5$ cells show the SET speed of ∼6 ns. Apparently, under lower bias, the $Ti_{0.4}Sb_2Te_3$ cell can complete the SET operation more quickly than the $Ti_1Sb_2Te_5$ cell. In contrast, the SET operation of $Ge_2Sb_2Te_5$ cell requires ∼75 ns at 1.6 V and ∼35 ns even at 2.1 V. In other words, one order of magnitude faster SET speed can still be achieved even by using the $Ti_1Sb_2Te_5$ cell. Supplementary Information Figure S1 shows the cell resistance versus required time curves for SET operation of such three cells.

In terms of the RESET operation, even the $Ti_{0.4}Sb_2Te_3$ (3.12 nJ) and $Ti_1Sb_2Te_5$ (1.65 nJ) cells with $D = 190$ nm BEC have noticeable lower energies compared to the $Ge_2Sb_2Te_5$ cells with smaller BEC (9.48 nJ for $D = 130$ nm BEC and 4.20 nJ for $D = 80$ nm BEC). More significant RESET energy reduction can be achieved on the $Ti_{0.4}Sb_2Te_3$ (0.95 nJ) and $Ti_1Sb_2Te_5$ (0.55 nJ) cells with $D = 80$ nm BEC. Namely, ∼78% and ∼87% of the energy have been saved via using the $Ti_{0.4}Sb_2Te_3$ and $Ti_1Sb_2Te_5$ cells ($D = 80$ nm BEC), respectively. Note that the $Ti_1Sb_2Te_5$ cell

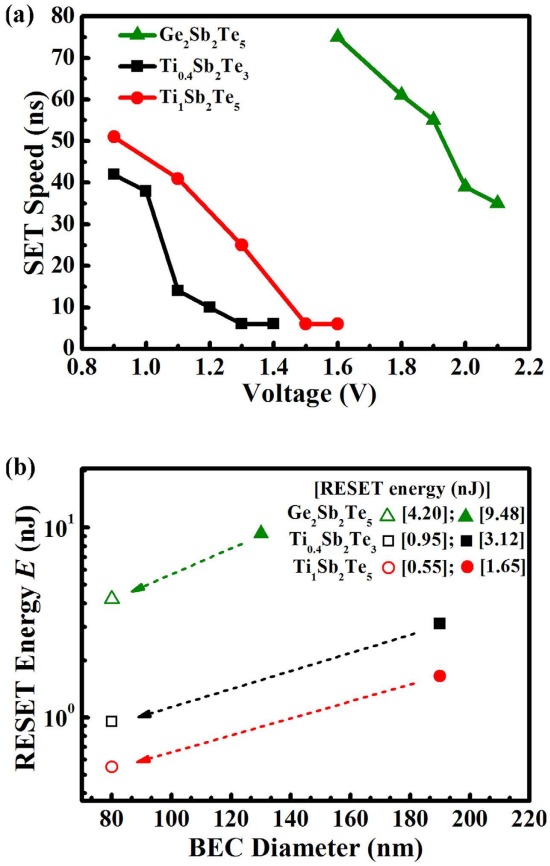

Figure 2. Comparisons of the SET operation speed and RESET energy. (**a**) SET operation speeds for the $Ge_2Sb_2Te_5$, $Ti_{0.4}Sb_2Te_3$, and $Ti_1Sb_2Te_5$ based PCM cells with the same $D = 190$ nm W BEC. (**b**) RESET energy as a function of BEC diameter D for the $Ge_2Sb_2Te_5$, $Ti_{0.4}Sb_2Te_3$, and $Ti_1Sb_2Te_5$ based PCM cells.

achieves a substantial (42∼47%) RESET energy reduction on the basis of the $Ti_{0.4}Sb_2Te_3$ cell. The shrinkage of BEC size also remarkably decreases the RESET current as shown in the Supplementary Information Figure S2. An ∼82% reduction of the RESET current is realized for both the $Ti_{0.4}Sb_2Te_3$ and $Ti_1Sb_2Te_5$ cells (∼0.5 mA) compared to that of $Ge_2Sb_2Te_5$ cell (∼2.8 mA) with the same $D = 80$ nm BEC. Moreover, the RESET current of the $Ti_1Sb_2Te_5$ cell (∼1.1 mA) is relatively smaller than that of the $Ti_{0.4}Sb_2Te_3$ cell (∼1.3 mA) with the same $D = 190$ nm BEC. In addition to the improvements in RESET energy and current, the endurance characteristics of the $Ti_1Sb_2Te_5$ cell (∼10^7 cycles) is not inferior to that of the $Ti_{0.4}Sb_2Te_3$ cell[7], which is obviously far more better than that of the $Ti_{0.56}Sb_2Te_3$ cell (<10^6 cycles with severe fluctuation of the RESET state)[9], as shown in the Supplementary Information Figure S3.

We used Raman spectroscopy (Fig. 3a) and *in situ* XRD (Fig. 3b) to characterize the c-$Ti_1Sb_2Te_5$ phase. As a CdI_2-like structure with space group $P\bar{3}m1$ space symmetry, c-$TiTe_2$ has two Raman active modes produced entirely by the Te atoms for both the in-plane, E_g peak (∼122 cm^{-1}), and out of plane, A_{1g} peak (∼143 cm^{-1}), with the Ti atoms at rest[15]. Since there is no distinctive shoulder near ∼160 cm^{-1}, the c-$TiTe_2$ film can be considered as a stoichiometric compound without noticeable defects or impurities[16]. Because c-Sb_2Te_3 crystal belongs to the space group $R\bar{3}m$, it has three Raman active modes, including two out of plane vibrations $A_{1g}(1)$ peak (∼69 cm^{-1}) and $A_{1g}(2)$ peak (∼165 cm^{-1}), and one in-plane vibration $E_g(1)$ peak (∼112 cm^{-1})[17]. Compared to the Raman curves of the c-$TiTe_2$ and c-Sb_2Te_3 films, the c-$Ti_1Sb_2Te_5$ film has five Raman active modes identically peaked corresponding to E_g and A_{1g} of $TiTe_2$ and $A_{1g}(1)$, $A_{1g}(2)$, and $E_g(1)$ of Sb_2Te_3, respectively, as shown in Fig. 3a. The coexistence of c-$TiTe_2$ and c-Sb_2Te_3 Raman active modes in c-$Ti_1Sb_2Te_5$ no doubt shall originate from the two separated phases which is already observed in c-$Ti_{0.4}Sb_2Te_3$[8]. In fact, our *in situ* XRD result of $Ti_1Sb_2Te_5$ film clearly proves such phase separation phenomenon as shown in Fig. 3b, where both HEX-Sb_2Te_3 and HEX-$TiTe_2$ diffraction peaks can be identified. Nevertheless we did not observe such distinct phase separation in $Ti_{0.4}Sb_2Te_3$ through the same *in situ* XRD measurement[7]. The phase separation in $Ti_{0.4}Sb_2Te_3$ occurs in nano-scale dimension[8], where the $TiTe_2$ lamellae segregate into no more than 10 nm-width belts and most of the $TiTe_2$ lamellae (<2 nm in width) inlay with the Sb_2Te_3 quintuple-layered blocks. Due to the similar HEX lattice structures of $TiTe_2$ and Sb_2Te_3, and also considering the lower doping content of Ti (∼7.4 at.%) in $Ti_{0.4}Sb_2Te_3$, less concentration of the $TiTe_2$ lamellae may result in undetected XRD signal. Note that the pure $TiTe_2$ alloy has quite high T_m (>1200 °C)[18] and the HEX-phase of its thin film can be maintained even at 700 °C (higher than the T_m ∼ 618 °C of Sb_2Te_3)[8], thus there is no segregated Te or Ti phase being observed in c-$Ti_1Sb_2Te_5$ as shown in Fig. 3b.

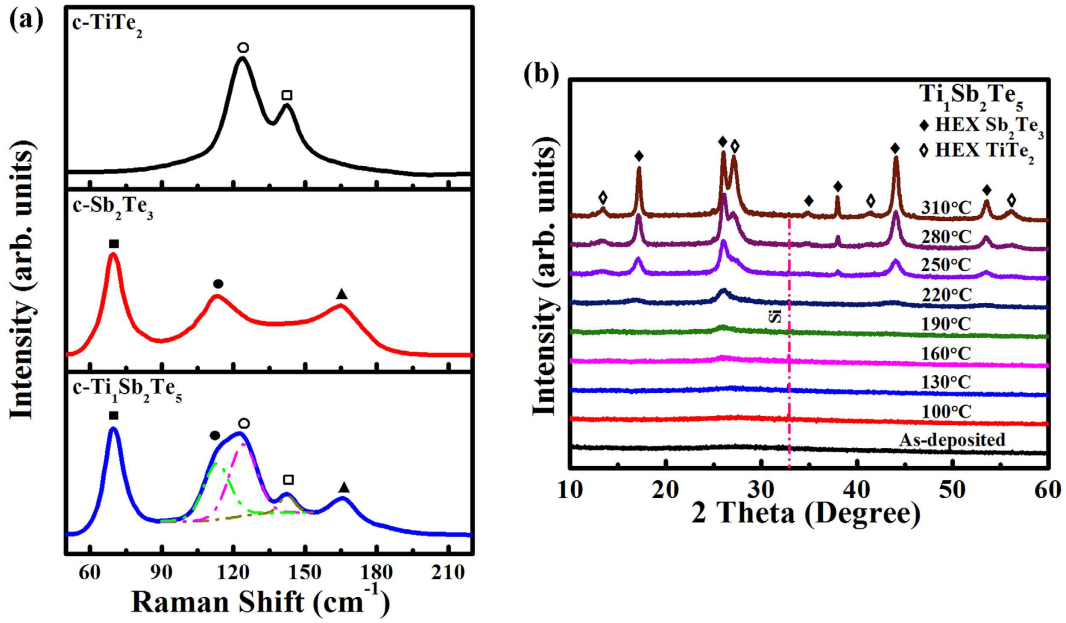

Figure 3. The Raman spectra of c-$TiTe_2$, c-Sb_2Te_3, and c-$Ti_1Sb_2Te_5$ and *in situ* XRD results of $Ti_1Sb_2Te_5$. (**a**) Raman spectra of the c-$TiTe_2$, c-Sb_2Te_3, and c-$Ti_1Sb_2Te_5$ films. One can see two main E_g (○) and A_{1g} (□) phonon modes for c-$TiTe_2$ film, and three main $A_{1g}(1)$ (■), $E_g(1)$ (●), and $A_{1g}(2)$ (▲) phonon modes for c-Sb_2Te_3 film. The c-$Ti_1Sb_2Te_5$ film shows all the five phonon modes. (**b**) *In situ* XRD curves of $Ti_1Sb_2Te_5$ film at different temperatures, where HEX lattice planes of Sb_2Te_3 (♦) and $TiTe_2$ (◊) can be identified.

Since the Ti dopants in c-$Ti_{0.4}Sb_2Te_3$ either segregate in the form of $TiTe_2$ lamellae or construct Ti-centered octahedrons scattered in the quintuple-layered blocks of the Sb-Te lattice[8], this non-stoichiometric composition can be chemically regarded as $(TiTe_2)_xTi_{0.4-x}Sb_2Te_{3-2x}$ $(0<x<0.4)$, where $(TiTe_2)_x$ part corresponds to the $TiTe_2$ lamellae and in $Ti_{0.4-x}Sb_2Te_{3-2x}$ part the $Ti_{0.4-x}Te_{0.8-2x}$ accounts for the scattered Ti-centered octahedrons. The $Ti_{0.4-x}Sb_2Te_{3-2x}$ part behaves more like the Sb-rich Sb-Te compound contributing to the faster recrystallization[8]. Extending this analysis to the stoichiometric $Ti_1Sb_2Te_5=(TiTe_2)_yTi_{1-y}Sb_2Te_{5-2y}$ $(0<y<1)$, where $(TiTe_2)_y$ part also stands for the segregated $TiTe_2$ lamellae, one can easily find that, in $Ti_{1-y}Sb_2Te_{5-2y}$ part $(=Ti_{1-y}Te_{2-2y}Sb_2Te_3)$, if $Ti_{1-y}Te_{2-2y}$ is assigned as the Ti-centered octahedrons accommodated in Sb-Te quintuple-layered blocks, it will be contradictory to keep the rest Sb-Te part in a ratio of 2 : 3 without Te deficiency. In other words, since there is no Ti or Te phase separation, it is more appropriate to describe the c-$Ti_1Sb_2Te_5$ as $(TiTe_2)_1(Sb_2Te_3)_1$ in which all the Ti atoms are supposed to be contained in the separated $TiTe_2$ lamellae. Of course, this is a rough estimate, however, we may still get a reasonable inference that compared to the c-$Ti_{0.4}Sb_2Te_3$, c-$Ti_1Sb_2Te_5$ should have a higher concentration of the c-$TiTe_2$ lamellae but a lower concentration of the "solid-solute" Ti-centered octahedrons.

Note that the quasi-two-dimensionalc-$TiTe_2$ is semimetallic[19] (see Fig. 1 also) with a quite low thermal conductivity (~0.12 W/mK)[20]. The $TiTe_2$ lamellae could act like the embedded nano-electrodes in c-$Ti_1Sb_2Te_5$ to conduct the electrical current to the adjacent Sb_2Te_3 grains to generate Joule heat. The heat dissipation could be concomitantly refrained by those low thermal-conductive $TiTe_2$ lamellae so as to effectively enhance the thermal efficiency of the RESET operation. Not surprisingly the c-$Ti_1Sb_2Te_5$ (~1/2 = 50.0% concentration of $TiTe_2$ lamellae) based PCM cell can accomplish substantial reduction of the RESET energy compared to the c-$Ti_{0.4}Sb_2Te_3$ ($< \sim 0.4/1.4 \approx 28.6\%$ concentration of $TiTe_2$ lamellae) based PCM cell. On the contrary, the lack of survived Ti-centered octahedrons in Sb-Te rich amorphous matrix after RESET operation may slow down the nucleation rate for recrystallization process[8,9], leading to a relatively slower SET speed for the $Ti_1Sb_2Te_5$ based PCM cell as compared to that of the $Ti_{0.4}Sb_2Te_3$ based one.

We also used the two-dimensional finite element method (FEM) to simulate and compare the RESET operations of the $Ge_2Sb_2Te_5$, $Ti_{0.4}Sb_2Te_3$, and $Ti_1Sb_2Te_5$ based PCM cells, as shown in Fig. 4. The Joule heat is mainly generated in the phase change films. The thermal transfer obeys the standard heat conduction equation:[21]

$$\nabla \cdot \kappa \nabla T + Q = \rho c \partial T / \partial t \quad (1)$$

where κ, is the thermal conductivity, c, the specific heat, ρ, the density, t, the time, T, the temperature, and Q, the Joule heat per unit volume and per unit time, which is called the heat density. The key material parameters for FEM simulations include κ of c-$Ge_2Sb_2Te_5$ (~0.46 W/mK)[21], c-Sb_2Te_3(~0.78 W/mK)[22], and c-$TiTe_2$ (~0.12 W/mK)[20], c of c-$Ge_2Sb_2Te_5$ (~1.20 J/cm^{3}K)[23], c-Sb_2Te_3(~1.02 J/cm^{3}K)[24], and c-$TiTe_2$ (assumed to be ~1.80 J/cm^{3}K of c-$TiSe_2$)[25], and ρ of c-$Ge_2Sb_2Te_5$ (~6.2 g/cm^3)[21], c-Sb_2Te_3 (~6.5 g/cm^3)[26], and c-$TiTe_2$ (~6.3 g/cm^3)[27]. The phase change film layers of the models are divided into grid shape to represent the poly-crystalline morphology. Each grid denotes the small crystal grain. ~29% and ~50% of the grids in the c-$Ti_{0.4}Sb_2Te_3$ and c-$Ti_1Sb_2Te_5$ layers are randomly chosen to be the c-$TiTe_2$ grains, respectively, as shown in Fig. 4b,c. Constant voltage pulse is applied to the axis-symmetric mushroom-type (T-shaped) cells. It can be observed the highest peak temperature is achieved

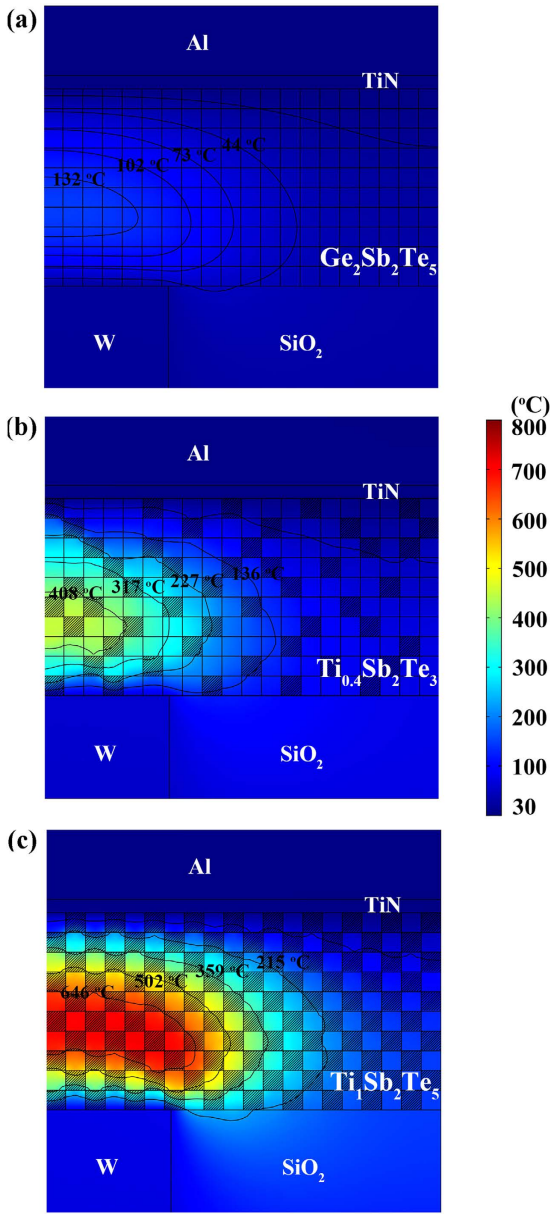

Figure 4. The two-dimensional finite element method simulations for the RESET operation. Simulated RESET temperature distributions in PCM cells with (**a**) c-$Ge_2Sb_2Te_5$, (**b**) c-$Ti_{0.4}Sb_2Te_3$, and (**c**) c-$Ti_1Sb_2Te_5$ layers. In (**a**) all the square grids represent the small $Ge_2Sb_2Te_5$ crystal grains, while in (**b**,**c**) the grids marked with slash lines stand for the $TiTe_2$ crystal grains, and other non-marked ones are belonged to the Sb_2Te_3 crystal grains. The isothermal curves with corresponding temperatures in the PCM cells are also shown.

in the $Ti_1Sb_2Te_5$ based cell (Fig. 4c) while the $Ge_2Sb_2Te_5$ based cell (Fig. 4a) has the lowest peak temperature. Apparently, more heat can be generated and confined in the phase change film layer as c-$TiTe_2$ concentration increases, therefore lower energy is needed for the RESET operation.

In summary, the pseudobinary $Ti_1Sb_2Te_5$ phase change alloy shows drastically decreased RESET energy, while increasing the SET speed, of the PCM cell compared to the $Ge_2Sb_2Te_5$ based one. Without significantly reducing the SET speed as compared to the $Ti_{0.4}Sb_2Te_3$ based PCM cell, nearly half of the RESET power can be saved on the $Ti_1Sb_2Te_5$ based one. These improvements are achieved by introducing more nano-scale separated $TiTe_2$ lamellae. We believe with more thermally stable $TiTe_2$ lamellae the efficiency of electric conduction and heat inhibition could be greatly enhanced for the low-energy RESET operation. We expect the speed/power to be further increased/decreased significantly on thorough investigations of the $(TiTe_2)_n(Sb_2Te_3)_m$ pseudobinary system and device dimension scaling techniques. In this regard, for example, a superlattice or multilayered structure constructed by alternate $TiTe_2/Sb_2Te_3$ stacking film instead of the co-sputtering one will be a great help. It may also be possible to search topological superconducting properties on a finely-tuned $TiTe_2/Sb_2Te_3$ superlattice sample.

Methods

$Ti_{0.4}Sb_2Te_3$ films were deposited by co-sputtering of pure Ti and Sb_2Te_3 targets. By adding an additional pure Te target, three-target co-sputtering technique was used to fabricate the $Ti_1Sb_2Te_5$ films. Similarly, $TiTe_2$ films were obtained by co-sputtering of pure Ti and Te targets. For Sb_2Te_3 and $Ge_2Sb_2Te_5$ films, respective pure alloy target was used for sputtering. The compositions of all films were measured by X-ray fluorescence spectroscopy using a Rigaku RIX 2100 system. The temperature-dependent sheet resistance changing trends of $TiTe_2$, Sb_2Te_3, $Ti_{0.4}Sb_2Te_3$, and $Ti_1Sb_2Te_5$ films with the same 150 nm thickness were studied by Linkam LMP 95 hot stage. For real-time observation of structure transition in $Ti_1Sb_2Te_5$ film, vacuum *in situ* X-ray diffraction (XRD) measurement with a 20 °C/min heating rate was performed on 300-nm-thick film (deposited on Si substrate at room temperature) using PANalytical X'Pert PRO diffractometer with a Cu Kα ($\lambda = 0.15418$ nm) radiation source. The diffraction data were collected in the 2θ range of 10°–60° with a scanning step of 0.02°. Raman spectroscopy (Thermo Fisher DXR) was performed on 300-nm-thick film samples at room temperature using an Ar^+ laser (wavelength 532 nm) with $\sim 1\,\mu m^2$ beam spot.

T-shaped PCM cells with diameter (D) = 190 (80) nm tungsten plug bottom electrode contact (BEC) were fabricated using 0.13 μm complementary metal-oxide semiconductor technology. In all the PCM cells, the thickness of the switching material films is around 170 nm. The 15-nm-thick TiN and 300-nm-thick Al films were used as top electrode for all cells. All the electrical measurements were performed by using the Keithley 2600C source meter (measuring cell resistance), the Tektronix AWG5002B pulse generator (generating voltage pulse with a minimum width of ~6 ns), the homemade constant current driver (generating current pulse with a maximum magnitude of ~10 mA), and the Tektronix 7054 digital phosphor oscilloscope (measuring transient voltage drop across the cell when current pulse is applied).

References

1. Lam, C. H. In Storage Class Memory. 10th IEEE International Conference onSolid-State and Integrated Circuit Technology. 1080–1083 (2010).
2. Frietas, R. F. & Wilcke, W. W. Storage-class memory: the next storage systemtechnology. *IBM J. Res. Dev*. **25,** 439 (2008).
3. Atwood, G. Phase-change materials for electronic memories. *Science* **321,** 210–211 (2008).
4. Wuttig, M. Phase-change materials: towards a universal memory? *Nat. Mater.* **4,** 265–266 (2005).
5. Kang, M. J. *et al.* PRAM cell technology and characterization in 20 nm node size. *IEEE International Electron Devices Meeting* **3,** 1.1–3.1.4 (2011).
6. Ahn, S. J. *et al.* Reliability perspectives for high density PRAM manufacturing. *IEEE International Electron Devices Meeting* **12,** 6.1–12.6.4 (2011).
7. Zhu, M. *et al.* One order of magnitude faster phase change at reduced power in Ti-Sb-Te. *Nat. Commun*. **5,** 4086 (2014).
8. Rao, F. *et al.* Direct observation of titanium-centered octahedral in titanium-antimony-tellurium phase-change material. *Nat. Commun*. **6,** 10040 (2015).
9. Xia, M. J. *et al.* Ti–Sb–Te Alloy: A candidate for fast and long-life phase-change memory. *ACS Appl. Mater. Inter.* **7,** 7627–7634 (2015).
10. Zhu, M. *et al.* The micro-structure and composition evolution of Ti-Sb-Te alloy during reversible phase transition in phase change memory. *Appl. Phys. Lett.* **104,** 063105 (2014).
11. Simpson, R. E., Fons, P., Kolobov, A. V., Krbal, M. & Tominaga, J. Enhanced crystallization of GeTe from an Sb_2Te_3 template. *Appl. Phys. Lett*. **100,** 021911 (2012).
12. Friedrich, I., Weidenhof, V., Njoroge, W., Franz, P. & Wuttig, M. Structural transformations of $Ge_2Sb_2Te_5$ films studied by electrical resistance measurements. *J. Appl. Phys.* **87,** 4130–4134 (2000).
13. Chung, K. M., Wamwangi, D., Woda, M., Wuttig, M. & Bensch, W. Investigation of SnSe, SnSe, and Sn_2Se_3 alloys for phase change memory applications. *J. Appl. Phys*. **103,** 083523 (2008).
14. Rao, F. *et al.* Investigation of changes in band gap and density of localized states on phase transition for $Ge_2Sb_2Te_5$ and $Si_{3.5}Sb_2Te_3$ materials. *Acta Mater.* **60,** 323–328 (2012).
15. Khan, J. M., Nolen, C. M., Teweldebrhan, D. & Balandin, A. A. Properties of quasi-two-dimensional crystals of titanium ditelluride. *ECS Transactions* **33,** 211–217 (2010).
16. Khan, J. M. *et al.* Anomalous electron transport in back-gated field-effect transistors with $TiTe_2$ semimetal thin-film channels. *Appl. Phys. Lett.* **100,** 043109 (2012).
17. Sosso, G. C., Caravati, S. & Bernasconi, M. Vibrational properties of crystalline Sb_2Te_3 from first principles. *J. Phys.: Condens. Matter*. **21,** 095410 (2009).
18. Cordes, H. & Schmid-Fetzer, R. Phase equilibria in the Ti-Te system. *J. Alloy.Compd*. **216,** 197–206 (1994).
19. Claessen, R. *et al.* Complete band-structure determination of the quasi-two-dimensional Fermi-liquid reference compound $TiTe_2$. *Phys. Rev. B* **54,** 2453–2465 (1996).
20. Chiritescu, C., Mortensen, C., Cahill, D. G., Johnson, D. & Zschack, P. Lower limit to the lattice thermal conductivity of nanostructured Bi_2Te_3-based materials. *J. Appl. Phys.* **106,** 073503 (2009).
21. Kang, D. H., Ahn, D. H., Kim, K. B., Webb, J. F. & Yi, K. W. One-dimensional heat conduction model for an electrical phase change random access memory device with an $8F^2$ memory cell ($F = 0.15\,\mu m$). *J. Appl. Phys*. **94,** 3536–3542 (2003).
22. Chen, J. *et al.* Sb_2Te_3 nanoparticles with enhanced Seebeck coefficient and low thermal conductivity. *Chem. Mater.* **22,** 3086–3092 (2010).
23. Kim, S. S. *et al.* Simulation for Reset operation of $Ge_2Sb_2Te_5$ phase-change random access memory. *Jpn. J. Appl. Phys.* **44,** 5943–5948 (2005).
24. Yáñez-Limón, J. M., González-Hernández, J., Alvarado-Gil, J. J., Delgadillo, I. & Vargas, H. Thermal and electrical properties of the Ge:Sb:Te system by photoacoustic and Hall measurements. *Phys. Rev. B* **52,** 16321–16324 (1995).
25. Craven, R. A., Di Salvo, F. J. & Hsu, F. S. L. Mechanisms for the 200 K transition in $TiSe_2$: A measurement of the specific heat. *Solid State Commun.* **25,** 39–42 (1978).
26. Anderson, T. L. & Krause, H. B. Refinement of the Sb_2Te_3 and Sb_2Te_2Se structures and their relationship to nonstoichiometric $Sb_2Te_{3-y}Se_y$ compounds. *Acta Crystallogr. B* **30,** 1307–1310 (1974).
27. McTaggart, F. K. & Wadsley, A. D. The sulphides, selenides, and tellurides of titanium, zirconium, hafnium, and thorium. I. Preparation and characterization. *Aust. J. Chem*. **11,** 445–457 (1958).

Acknowledgements

This work was supported by Strategic Priority Research Program of Chinese Academy of Sciences (XDA09020402), National Integrate Circuit Research Program of China (2009ZX02023-003), National Natural

Science Foundation of China (61076121, 61176122, 61106001, 61261160500, 61376006), Science and Technology Council of Shanghai (13ZR1447200, 13DZ2295700).

Author Contributions

K.D. prepared the film samples and carried out the *in situ* XRD, Raman measurements and so on. K.D., L.W. and Y.C. fabricated the PCM cells and carried out electrical measurements. S.L. prepared PCM cell TEM samples by using FIB technique. F.R. carried out theoretical analysis and wrote this paper with help from all co-authors. The project was initiated and conceptualized by F.R. and Z.S.

Additional Information

Supplementary information accompanies this paper at http://www.nature.com/srep

Competing financial interests: The authors declare no competing financial interests.

How to cite this article: Ding, K. *et al.* Low-Energy Amorphization of $Ti_1Sb_2Te_5$ Phase Change Alloy Induced by $TiTe_2$ Nano-Lamellae. *Sci. Rep.* **6**, 30645; doi: 10.1038/srep30645 (2016).